Front. Energy 2020, 14(3): 649–665
https://doi.org/10.1007/s11708-018-0548-0

RESEARCH ARTICLE

Mohammad Reza NAZEMZADEGAN, Alibakhsh KASAEIAN, Somayeh TOGHYANI, Mohammad Hossein AHMADI, R. SAIDUR, Tingzhen MING

Multi-objective optimization in a finite time thermodynamic method for dish-Stirling by branch and bound method and MOPSO algorithm

Abstract There are various analyses for a solar system with the dish-Stirling technology. One of those analyses is the finite time thermodynamic analysis by which the total power of the system can be obtained by calculating the process time. In this study, the convection and radiation heat transfer losses from collector surface, the conduction heat transfer between hot and cold cylinders, and cold side heat exchanger have been considered. During this investigation, four objective functions have been optimized simultaneously, including power, efficiency, entropy, and economic factors. In addition to the four-objective optimization, three-objective, two-objective, and single-objective optimizations have been done on the dish-Stirling model. The algorithm of multi-objective particle swarm optimization (MOPSO) with post-expression of preferences is used for multi-objective optimizations while the branch and bound algorithm with pre-expression of preferences is used for single-objective and multi-objective optimizations. In the case of multi-objective optimizations with post-expression of preferences, Pareto optimal front are obtained, afterward by implementing the fuzzy, LINMAP, and TOPSIS decision making algorithms, the single optimum results can be achieved. The comparison of the results shows the benefits of MOPSO in optimizing dish Stirling finite time thermodynamic equations.

Keywords dish-Stirling, finite time model, branch and bound algorithm, multi-objective particle swarm optimization (MOPSO)

Received Mar. 3, 2017; accepted Jun. 1, 2017; online Apr. 6, 2018

Mohammad Reza NAZEMZADEGAN, Alibakhsh KASAEIAN, Somayeh TOGHYANI
Department of Renewable Energies, Faculty of New Science and Technologies, University of Tehran, Tehran, 1417466191, Iran

Mohammad Hossein AHMADI (✉)
Faculty of Mechanical Engineering and Mechatronic, Shahrood University of Technology, Shahrood 3619995161, Iran
E-mail: mohammadhosein.ahmadi@gmail.com

R. SAIDUR
Faculty of Science and Technology, Sunway University, No. 5, Jalan Universiti, Bandar Sunway, 47500 Petaling Jaya, Malaysia; Department of Engineering, Lancaster University, Lancaster, LA1 4YW, UK

Tingzhen MING
School of Civil Engineering and Architecture, Wuhan University of Technology, Wuhan 430070, China

1 Introduction

The energy crisis and environmental concerns at the late 20th century drew the attention of worldwide societies to fossil fuels replacements. One of the most important replacements of fossil fuels is solar energy [1]. Dish-Stirling systems by implementing solar energy in the Stirling cycle are one of the most-known solar systems. There are various analyses for a solar system with the dish-Stirling technology. One of those analyses is the finite time analysis. The finite time models were first attained by Curzon and Ahlborn [2]. After about 20 years that this model had been utilized, some researchers questioned the applicability of the finite time models [3,4]. One of the reasons of not trusting the finite time model is the reversibility assumption that has been considered in this model. Therefore, the results of the model have been different from the experimental results. To improve this error, a new parameter called the irreversibility factor was developed. In some papers, including the research done by Tlili [5], the benefits of this parameter was studied. In another work conducted by Urieli et al., this parameter was considered in the model [6–10].

There are many researches about Stirling engines and their cycles. Wu et al. [11] considered the regenerator and heat exchanger irreversibilities of Stirling engines. They

also developed a correlation between the total output power and the thermal efficiency. Petrescu et al. conducted an analysis based on the first law of thermodynamics with direct method and the finite speed model on a close cycle and calculated the power and efficiency of the Stirling engine [12]. Timoumi et al. [13] for the purpose of increasing the efficiency of the Stirling engine, analyzed the second order Stirling engine and some physical and geometrical parameters in the engine efficiency. Cheng and Yu [14] developed a numerical model for a Beta type Stirling engine. They considered the non-isothermal effects, the regenerator performance, and the heater thermal resistance. They also predicted the periodic changes in the pressure, volume, temperature, heat transfer, and mass transfer rates of the system.

Ataer [15] studied a free-piston Stirling engine. In this model, the piston replacement parameter was used and therefore, time was eliminated from the equations. Tlili [16], in one of his researches, maximized the output power and efficiency of an internal reversible heat engine at the maximum point of power. He considered the regenerator loss in his study. Formosa and Despesse performed a thermodynamic analysis on a free-piston Stirling engine. They used the experimental data of a GPU-3 engine in their model [17]. Formosa studied a free-piston Stirling engine with a thermodynamic-dynamic semi-analytical model in another work [18]. Some researchers did different works about Stirling engines, Stirling cycles, and dish-Stirling systems. The comparison of low and high temperature differential Stirling engines, investigation of solar collector design parameters, and study of a real engine were included in these works [19–21].

Besides the analyses that have been done about Stirling engines and cycles, there were some works which optimized the Stirling cycles [22,23]. In some of these papers, the simultaneous optimization of more than one objective function was observed. This type of optimization, called multi-objective optimization, basically used the artificial intelligence methods to achieve the optimum solution. One of the most popular methods used in Stirling cycle optimizations was the genetic algorithm [24–32]. The genetic algorithm is a type of evolutionary algorithm. In addition, some energy system optimizations were done using the particle swarm optimization (PSO) methods. For example, Chaitou and Nika optimized a thermoacoustic engine [33]. In some of the optimizations, the multi-objective particle swarm optimization (MOPSO) algorithm was used for optimizing the Stirling cycles [34,35].

Most of the multi-objective optimizations done in the previous studies were with post-expression of preferences, and the algorithms implemented in these studies were usually with three or less objective functions. In this investigation, four objective functions are optimized simultaneously, including the power, efficiency, entropy, and economic factors. In addition to the four-objective optimization, the three-objective, the two-objective, and the single-objective optimizations are carried out on the dish-Stirling model. In this study, the algorithm of MPOSO with post-expression of preferences is used for multi-objective optimizations while the branch and bound algorithm with pre-expression of preferences is used for single-objective and multi-objective optimizations. In the case of multi-objective optimizations with post-expression of preferences, after obtaining the Pareto optimal front by implementing the fuzzy, LINMAP, and TOPSIS decision making algorithms, the single optimum results can be achieved.

2 Methodology

In dish-Stirling systems, parabolic mirrors reflect solar light through a collector which reflects the radiation on the hot side of Stirling engine. In the present system, it is assumed that the dish is equipped with a sun tracker. Therefore, at any moment, the maximum possible solar energy reaches the collector. In addition to the hot side, there is a cold side or heat sink in the Stirling engine. In this study, it is assumed that the hot side and cold side have constant temperatures.

As shown in Fig. 1, the Stirling thermodynamic cycle consists of two isothermal and two constant-volume processes. In process 1–2, a compressing working fluid at a constant temperature of T_c rejects the heat to a heat sink at a constant temperature of T_L. In process 2–3, the working fluid crosses over the regenerator in an isochoric process and is preheated to the temperature of T_h. In process 3–4, the working fluid receives the heat from the heat source and expands through an isothermal process with a temperature of T_H. In process 4–1, the working fluid cools down through a constant-volume process by the regenerator.

By considering the convection and radiation heat losses,

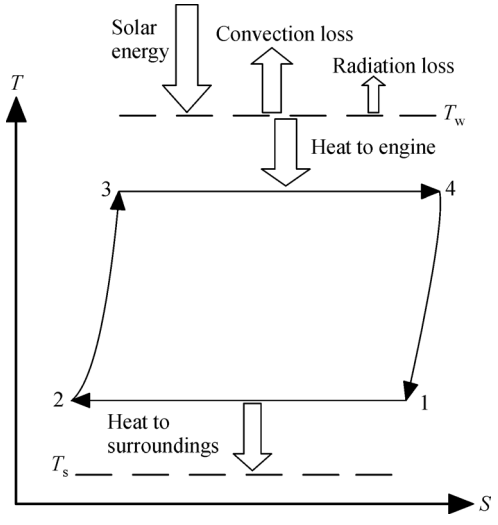

Fig. 1 Thermodynamic cycle of Stirling

the useful thermal energy received may be calculated by Eq. (1).

$$q_u = IA_{app}\eta_0 - A_{rec}[h(T_H - T_0) + \varepsilon\delta(T_H^4 - T_0^4)], \quad (1)$$

where I is direct solar flux intensity and A_{app} is collector aperture area.

The thermal efficiency of the dish-Stirling system can be calculated by

$$\eta_s = \frac{q_u}{IA_{app}} = \eta_0 - \frac{1}{IC}\left[h(T_H - T_0) + \varepsilon\delta\left(T_H^4 - T_0^4\right)\right], \quad (2)$$

where C is collector concentration ratio.

The heat transferred at the hot side and the cold side of the Stirling cycle can be calculated by Eqs. (3) and (4).

$$Q_h = [h_h A_H (T_H - T_h)]t_h, \quad (3)$$

$$Q_c = [h_c A_L (T_c - T_L)]t_l, \quad (4)$$

where t_h and t_l are the duration times of the heat transfer process at the hot side and the cold side, respectively.

By implementing the thermodynamic equations and the entropy definition, the heat that is transferred at the hot side of the cycle may be calculated by Eq. (5). Also, by considering the irreversibility factor (ϕ), the rate of heat transfer at the cold side of the cycle is calculated by Eq. (6). It is worthy to mention that the irreversibility factor can be greater than or equal to one.

$$Q_{34} = Q_h = nRT_h \ln\left(\frac{V_4}{V_3}\right) = nRT_h \ln\lambda, \quad (5)$$

$$Q_c = \phi nRT_c \ln\left(\frac{V_1}{V_2}\right) = \phi nRT_c \ln\lambda. \quad (6)$$

By simultaneously using the thermodynamic and heat transfer equations, the duration time of each Stirling cycle process can be calculated. By utilizing Eqs. (3) and (5), the duration time of process 3–4 may be obtained throug Eqs. (7) and (8).

$$[h_h A_H (T_H - T_h)]t_h = nRT_h \ln\lambda, \quad (7)$$

$$t_h = \frac{nRT_c \ln\lambda}{[h_h A_H (T_H - T_h)]}. \quad (8)$$

Also, by applying Eqs. (4) and (6), the time of heat transfer at the cold side can be calculated by Eqs. (9) and (10).

$$[h_c A_L (T_c - T_L)]t_l = \phi nRT_c \ln\lambda, \quad (9)$$

$$t_l = \frac{\phi nRT_c \ln\lambda}{[h_c A_L (T_c - T_L)]}. \quad (10)$$

To calculate the time of regenerator processes, Eq. (11) can be used.

$$\frac{dT}{dt} = \pm M_i, \quad (11)$$

where M is only a function of property of the regenerator materials and called the regenerative time constant. In this regard, the time of processes 2–3 and 4–1 can be calculated by Eqs. (12) and (13).

$$t_3 = \frac{T_h - T_c}{M_1}, \quad (12)$$

$$t_4 = \frac{T_h - T_c}{M_2}. \quad (13)$$

Therefore, according to Eqs. (7) to (13), the total time of the whole thermodynamic cycle can be obtained by Eq. (14).

$$t = \frac{nRT_h \ln\lambda}{[h_h A_H (T_H - T_h)]} + \frac{\phi nRT_c \ln\lambda}{[h_c A_L (T_c - T_L)]} + \frac{T_h - T_c}{M_1} + \frac{T_h - T_c}{M_2}. \quad (14)$$

2.1 Heat loss between the hot and cold cylinders of the Stirling engine

Due to the low distance between the hot and cold cylinders of the Stirling engine, there is an undesirable conduction heat transfer between the two cylinders. This heat loss can be calculated by Eq. (15).

$$Q_0 = k_0(T_H - T_L)t. \quad (15)$$

By considering this heat loss, the total heat removed from the heat source and the total heat absorbed by the heat sink may be estimated by Eqs. (16) and (17).

$$Q_H = Q_h + Q_0, \quad (16)$$

$$Q_L = Q_c + Q_0. \quad (17)$$

2.2 Power, thermodynamic efficiency, and entropy calculation

To calculate the power, thermodynamic efficiency, and entropy change of the cycle, Eqs. (18) to (20) can be utilized.

$$P' = \frac{W}{t} = \frac{Q_H - Q_L}{t}, \quad (18)$$

$$\eta_t = \frac{Q_H - Q_L}{Q_H}, \quad (19)$$

$$\sigma = \frac{1}{t}\left(\frac{Q_L}{T_L} - \frac{Q_H}{T_H}\right). \quad (20)$$

By implementing a variable changing as shown in Eq. (21), Eqs. (22) to (24) are achieved.

$$F_1 = \frac{1}{nR\ln\lambda}\left(\frac{1}{M_1} + \frac{1}{M_2}\right), \tag{21}$$

$$P' = \frac{T_h - \phi T_c}{\left(\frac{T_h}{[h_h A_H (T_H - T_h)]} + \frac{\phi T_c}{[h_c A_L (T_c - T_L)]} + F_1 (T_h - T_c)\right)}, \tag{22}$$

$$\eta_t = \frac{T_h - \phi T_c}{T_h + k_0 (T_H - T_L)\left(\frac{T_h}{[h_h A_H (T_H - T_h)]} + \frac{\phi T_c}{[h_c A_L (T_c - T_L)]} + F_1 (T_h - T_c)\right)}, \tag{23}$$

$$\sigma = \frac{\left(\frac{\phi T_c}{T_L} - \frac{T_h}{T_H}\right)}{\left(\frac{T_h}{[h_h A_H (T_H - T_h)]} + \frac{\phi T_c}{[h_c A_L (T_c - T_L)]} + F_1 (T_h - T_c)\right)}. \tag{24}$$

Also, by utilizing two new parameters as $x = (T_c/T_h)$ and $A_R = (A_L/A_H)$, the power, efficiency and entropy change may be obtained by Eqs. (25) to (27).

$$P' = \frac{1 - \phi x}{\frac{1}{[h_h A_H (T_H - T_h)]} + \frac{\phi x}{[h_c A_R A_H (x T_h - T_L)]} + F_1 (1 - x)}, \tag{25}$$

$$\eta_t = \frac{1 - \phi x}{1 + k_0 (T_H - T_L)\left(\frac{1}{[h_h A_H (T_H - T_h)]} + \frac{\phi x}{[h_c A_R A_H (x T_h - T_L)]} + F_1 (1 - x)\right)}, \tag{26}$$

$$\sigma = \frac{\left(\frac{\phi x}{T_L} - \frac{1}{T_H}\right)}{\frac{1}{[h_h A_H (T_H - T_h)]} + \frac{\phi x}{[h_c A_R A_H (x T_h - T_L)]} + F_1 (1 - x)}. \tag{27}$$

By having the thermal efficiency of the solar mirror and the thermodynamic efficiency of the Stirling engine, the total efficiency of the dish-Stirling system can be achieved by Eq. (28).

$$\eta_m = \eta_t \eta_s. \tag{28}$$

2.3 Economic factor

The economic factor in the dish-Stirling equations shows the power output of the system per unit of investment cost. This definition actually has been replaced with the definition of power per unit of fuel in many energy systems; but since there is no fuel in a solar system, the economic factor has been defined [30]. The economic factor is described by Eq. (29).

$$F' = \frac{P'}{C_{ai}}. \tag{29}$$

The investment of the dish-Stirling system itself is a function of the heat transfer area of the hot and cold sides of the cycle [30]. This function is shown in Eq. (30).

$$C_{ai} = aA_H + bA_L. \tag{30}$$

2.4 Objective functions

By substituting Eqs. (25) to (30) in Eq. (29) and utilizing the following variable changing, Eq. (32) can be driven. Also, by implementing some variable changes as Eqs. (33) to (35), finally the dimensionless objective functions can be achieved as Eqs. (36) to (39).

$$z=\frac{a}{a+b}, \tag{31}$$

$$F'=\frac{1-\phi x}{a\left(\frac{1+\left(\frac{1-z}{z}\right)A_{\mathrm{R}}}{[h_{\mathrm{h}}(T_{\mathrm{H}}-T_{\mathrm{h}})]}+\frac{\phi x\left(1+\left(\frac{1-z}{z}\right)A_{\mathrm{R}}\right)}{[h_{\mathrm{c}}A_{\mathrm{R}}(xT_{\mathrm{h}}-T_{\mathrm{L}})]}+F_1(1-x)\left(1+\left(\frac{1-z}{z}\right)A_{\mathrm{R}}A_{\mathrm{H}}\right)\right)}, \tag{32}$$

$$f=\frac{aF'}{h_{\mathrm{h}}T_{\mathrm{L}}}, \tag{33}$$

$$P=\frac{P'}{h_{\mathrm{h}}A_{\mathrm{h}}T_{\mathrm{L}}}, \tag{34}$$

$$S=\frac{\sigma}{h_{\mathrm{h}}A_{\mathrm{h}}T_{\mathrm{L}}}, \tag{35}$$

$$f=\frac{1-\phi x}{T_{\mathrm{L}}\left(\frac{1+\left(\frac{1-z}{z}\right)A_{\mathrm{R}}}{(T_{\mathrm{H}}-T_{\mathrm{h}})}+\frac{\phi x h_{\mathrm{h}}\left(1+\left(\frac{1-z}{z}\right)A_{\mathrm{R}}\right)}{h_{\mathrm{c}}A_{\mathrm{R}}(xT_{\mathrm{h}}-T_{\mathrm{L}})}+F_1h_{\mathrm{h}}A_{\mathrm{H}}(1-x)\left(1+\left(\frac{1-z}{z}\right)A_{\mathrm{R}}\right)\right)}, \tag{36}$$

$$P=\frac{1-\phi x}{T_{\mathrm{L}}\left(\frac{1}{(T_{\mathrm{H}}-T_{\mathrm{h}})}+\frac{\phi x h_{\mathrm{h}}}{h_{\mathrm{c}}A_{\mathrm{R}}(xT_{\mathrm{h}}-T_{\mathrm{L}})}+F_1h_{\mathrm{h}}A_{\mathrm{H}}(1-x)\right)}, \tag{37}$$

$$\eta_{\mathrm{m}}=\left(\eta_0-\frac{1}{IC}\left[h(T_{\mathrm{H}}-T_0)+\varepsilon\delta\left(T_{\mathrm{H}}^4-T_0^4\right)\right]\right)\frac{1-\phi x}{1+k_0(T_{\mathrm{H}}-T_{\mathrm{L}})\left(\frac{1}{[h_{\mathrm{h}}A_{\mathrm{H}}(T_{\mathrm{H}}-T_{\mathrm{h}})]}+\frac{\phi x}{[h_{\mathrm{c}}A_RA_{\mathrm{H}}(xT_{\mathrm{h}}-T_{\mathrm{L}})]}+F_1(1-x)\right)}, \tag{38}$$

$$S=\frac{\left(\frac{\phi x}{T_{\mathrm{L}}}-\frac{1}{T_{\mathrm{H}}}\right)}{T_{\mathrm{L}}\left(\frac{1}{(T_{\mathrm{H}}-T_{\mathrm{h}})}+\frac{\phi x h_{\mathrm{h}}}{h_{\mathrm{c}}A_{\mathrm{R}}(xT_{\mathrm{h}}-T_{\mathrm{L}})}+F_1h_{\mathrm{h}}A_{\mathrm{H}}(1-x)\right)}. \tag{39}$$

3 Variables constraints

After achieving the dimensionless objective functions, the next step is to specify the decision variables ranges. According to the final form of the objective functions, the decision variables consist of φ (internal irreversibility factor), A_{R} (cold side area to hot side area ratio of Stirling cycle), x (cold temperature to hot temperature ratio of working fluid), T_{H} (hot side temperature of the cycle) and T_{h} (hot temperature of working fluid). These variables are the most important variables from the system operation point of view. Afterward, values of other parameters will be specified.

The optimization will be done with the following constraints. Equations (40) to (44) show the variable constraints.

$$\phi\geqslant 1, \tag{40}$$

$$0.45\leqslant x\leqslant 0.7, \tag{41}$$

$$0.25\leqslant A_{\mathrm{R}}\leqslant 10, \tag{42}$$

$$1100\leqslant T_{\mathrm{H}}\leqslant 1400, \tag{43}$$

$$850\leqslant T_{\mathrm{h}}\leqslant 1000. \tag{44}$$

4 Multi-objective optimization

There are various definitions for multi-objective optimization in economy and engineering; but there are some common basic concepts in all of its definitions. Some of these basic concepts consist of the preferences, the utility function, and the Pareto optimal front [36–38].

Preferences: It is about preferences of decision maker in choosing the optimum point. There are two main types of preferences in multi-objective optimization. One preference takes into consideration the objective function before optimization, e.g., by inserting some coefficient into objective functions and adding the objective functions to each other and creating a main objective function, the so called utility function. In this paper, this type of preference is referred to as the pre-expression of preferences. In the other type, the decision making process is utilized after achieving the results. In this step, there is not a single point as the optimum point; but a series of non-dominated points make a frontier, which is called the Pareto frontier or the Pareto optimal front. Therefore, by implementing an appropriate decision making algorithm which applies the preferences of decision maker, the single optimum point will be achieved. In this paper, this type of preference is referred to as the post-expression of preferences.

Utility function: It considers the decision maker satisfaction. In pre-expression of preferences multi-objective optimization, one utility function is defined for each objective function that shows the related importance of each objective function. The combination of utility functions makes the main utility function.

Pareto optimal front: In post-expression of preferences multi-objective optimization, the results of the first step are a series of points. The Pareto optimal front includes a group of those points, the so called non-dominated points. The non-dominated points are the points that, in comparison with every other point at least at one objective function, are closer to the optimum result of that objective function. By implementing the decision making algorithms at the Pareto frontier, the ultimate optimum result can be achieved.

The particle swarm algorithm was first introduced by Kennedy and Eberhart [39]. The beginning of this algorithm is inspired by the studies done on the movements of birds and fishes in groups. According to the studies, the movements of each fish in its group are affected by the best pervious movements of its own and every other fishes in the group where the best movement means, for example closer approach to the food. Therefore, there is a direct or indirect relation between the movements of each fish in the group. By passing the time and repeating the movements, finally all of the fishes are closer to the food, in comparison to the first movements.

For the particle swarm algorithm there is also a similar procedure. In the particle swarm optimization (PSO), a random group of particles are chosen. Each particle represents one point in the result area. There is a memory for each point, which makes the point move toward its previous best position and the best positions of all other particles. At the end, by enough iteration, the best position of particles can be found in an acceptable neighborhood of the optimum point.

The best previous position of each particle is called personal optimum and the best previous position of all particles is called the overall optimum. If a movement and a position vector for each particle are considered, the next movement vector and the next position vector of each point would be driven by the influence of these four factors: the present position vector, the present movement vector, the difference between present position vector and the personal optimum, and the difference between present position vector and the overall optimum.

5 Decision making algorithms

As mentioned before, the results of multi-objective optimizations with post-expression of preferences make the Pareto optimal front. After developing the Pareto frontier, by utilizing decision making algorithms, the ultimate optimum point would be achieved. To obtain the optimum result, there are so many decision making algorithms, but the three most popular of these algorithms are fuzzy, TOPSIS, and LINMAP. In this study these three decision making algorithms have been considered.

Before implementing the decision making algorithms into the Pareto frontier, the results of the previous step of optimization should be non-dimensionalized. Two non-dimentionalization methods are described here.

(a) Linear non-dimensionalization

The results of multi-objective optimization are vectors with more than one dimension. The number of dimensions of multi-objective optimization results is as many as the number of objective functions. If a point of Pareto frontier is presented by F_{ij}, where i is the index for each point and j is the index for each objective function, the linear non-dimensionalization algorithm for a point when its objective is maximizing or minimizing is shown by Eqs. (45) and (46), respectively.

$$F_{ij}^{\text{norm}} = \frac{F_{ij}}{\max_i(F_{ij})}, \tag{45}$$

$$F_{ij}^{\text{norm}} = \frac{F_{ij}}{\max_i\left(\frac{1}{F_{ij}}\right)}. \tag{46}$$

(b) Fuzzy non-dimensionalization

In this method, for each point of F_{ij}, the distance to the ideal point is divided by the distance between the ideal

point and the non-ideal point. The ideal point is the point in which all of the objective functions are optimum and the non-ideal point is the point in which all of the objective functions are the worst possible amount. According to that, in the multi-objective optimization, the results have been achieved by trial and error so that the worst possible amount of each objective has a specific value. The fuzzy non-dimensionalization of point F_{ij} can be calculated by Eq. (47).

$$F_{ij}^{\text{norm}} = \frac{F_{ij} - F_{ij}^{\text{nonideal}}}{F_{ij}^{\text{ideal}} - F_{ij}^{\text{nonideal}}}. \quad (47)$$

5.1 Fuzzy decision making method

In this method, the dimensionless values that are non-dimensionalized by the fuzzy method, are utilized. As mentioned before, in the non-dimensionalization step, there is a corresponding dimensionless point for any point at the Pareto frontier. In the fuzzy decision making method, for each dimensionless point of F_{ij}, the optimum point is achieved by Eq. (48).

$$F_{\text{OptFuzzy}} = F_{ij};\max_i \left[\min_j \left(\frac{F_{ij} - F_{ij}^{\text{nonideal}}}{F_{ij}^{\text{ideal}} - F_{ij}^{\text{nonideal}}} \right) \right]. \quad (48)$$

5.2 LINMAP decision making algorithm

The basic of this method is about finding a point in the Pareto optimal front that is closest to the ideal point. This method can be expressed by Eq. (49).

$$F_{\text{OptLinmap}} = F_{ij};\min(|F^{\text{Ideal}} - F|). \quad (49)$$

5.3 TOPSIS decision making algorithm

This algorithm is based on finding a point in the Pareto frontier that has the least distance to the ideal point and the most distance to the non-ideal point. In fact, this is the point whose distance to the ideal point minus its distance to the non-ideal point is minimum in comparison to all other Pareto points. This method can be expressed by Eq. (50).

$$F_{\text{OptTopsis}} = F_{ij};\min(|F^{\text{Ideal}} - F\ | - |F^{\text{nonIdeal}} - F|). \quad (50)$$

Afterward, first the set values of parameters will be specified and then the results of optimizations of dish-Stirling system will be presented.

Optimization parameters

With the purpose of optimization of the dish-Stirling model, the values of constant parameters should be specified. To have consistency with previous studies, the specific value of parameters are considered as follows [22,30]:

$h_h = h_c = 200\ \text{W}\cdot\text{K}^{-1}\cdot\text{m}^{-2}$, $f = 0.7$, $C = 1300$, $\delta = 5.67 \times 10^{-8}\text{W}\cdot\text{K}^{-4}\cdot\text{m}^{-2}$, $T_L = 300$ K, $h = 20\ \text{W}\cdot\text{K}^{-1}\cdot\text{m}^{-2}$, $I = 1000\ \text{W}\cdot\text{m}^{-2}$, $(1/M_1 + 1/M_2) = 2\times10^{-5}\ \text{s.K}^{-1}$, $R = 8.3\ \text{J}\cdot\text{mol}^{-1}\cdot\text{K}^{-1}$, $n = 1$ mol, $\lambda = 2$, $\varepsilon = 0.9$, $k_0 = 2.5\ \text{W}\cdot\text{K}^{-1}$, $\eta_0 = 0.85$.

6 Results

As mentioned before, at the present study, the dish-Stirling model is solved in the cases of single-objective and multi-objective optimizations. In the case of multi-objective optimizations, there are two types of pre-expression and post-expression of preferences. In the case of optimization with pre-expression of preferences, there is a four-objective optimization. But in the case of optimization with post-expression of preferences, there appear two-objective, three-objective, and four-objective optimizations. Finally, the results of all these optimizations are presented.

6.1 Results of single-objective optimization

For each one of the four objective functions, there is an optimum point. To optimize each objective function, the branch and bound optimization algorithm has been utilized. The branch and bound algorithm is a nonlinear optimization. Table 1 lists the optimum results for each objective function together with corresponding values of other objective functions.

6.2 Results of four-objective optimization with pre-expression of preferences

By using the branch and bound algorithm in order to solve the four-objective optimization with pre-expression of preferences, the results of optimization of the dish-Stirling model are presented in Table 2.

Table 1 Results of single-objective optimization

	Decision variables					Objectives			
	φ	x	A_R	T_H	T_h	f	P	η	S
Max(f)	1.000	0.478	1.491	1400.0	998.290	0.190	0.312	0.333	0.000465
Max(P)	1.000	0.475	10.000	1400.0	850.000	0.100	0.531	0.344	0.000790
Max(η)	1.000	0.450	10.000	1100.0	850.000	0.060	0.315	0.408	0.000285
Min(S)	1.000	0.450	0.250	1100.0	850.000	0.046	0.051	0.323	0.000046

Table 2 Results of four-objective optimization with pre-expression of preferences

Decision variables					Objectives			
φ	x	A_R	T_H	T_h	f	P	η	S
1.000	0.450	10.000	1400.0	876.6	0.100	0.528	0.36	0.000665

In this optimization, each of the four objective functions have a proportional weight to their optimum value.

6.3 Results of multi-objective optimization with post-expression of preferences

As mentioned before, in the case of optimization with post-expression of preferences, there are two-objective, three-objective, and four-objective optimizations.

6.3.1 Four-objective optimization results

Since there are four objective functions, the results of this optimization are vectors with four dimensions. Therefore, the results cannot be shown in a chart and due to the great number of results, just the ultimate optimum result is presented in this case. The ultimate result, achieved by each one of the decision making methods, is presented in Table 3.

According to the results of four-objective optimization, at the ultimate optimal point, the dimensionless power is in the range of 0.33 to 0.34 and the thermal efficiency falls in the range of 0.35 to 0.37. Among the decision making algorithms, the fuzzy algorithm has picked an optimal point with the best thermal efficiency and slightly more optimum entropy. On the other hand, an optimal point with a better economical factor has been chosen by the TOPSIS algorithm.

6.3.2 Three-objective optimization results

By having four objective functions, there could be four optimizations of three-objective optimization. Therefore, the Pareto frontier and ultimate optimum results of each three-objective optimization are presented in Figs. 2–5 and Tables 3–6. In Section 6, the figures represent the corresponding Pareto frontier. In these figures the non-dominating points, the ideal point, the non-ideal point, and the ultimate optimal point, chosen by the decision making algorithms, have been shown. Besides, the tables in this section represent the optimal objective functions and their corresponding decision variables chosen by various decision making algorithms.

The results of the economic factor, the power, and the thermal efficiency of the three-objective optimization are demonstrated in Fig. 2 and Table 4. According to these results and in comparison with other decision making methods, the fuzzy algorithm, the LINMAP algorithm, and the TOPSIS algorithm have reached the best thermal efficiency, power, and economic factor, respectively.

Figure 3 and Table 5 display the results of the economic factor, the power, and the entropy of the three-objective optimization. The interesting point in these results is that both the LINMAP and the TOPSIS algorithm have obtained a similar optimal point.

The results of the economic factor, the thermal efficiency, and the entropy of the three-objective optimization are shown in Fig. 4 and Table 6. The results show that all of three decision making algorithms have obtained similar optimal points, although the fuzzy algorithm has obtained a better economic factor and thermal efficiency.

Figure 5 and Table 7 represent the results of the power, the thermal efficiency, and the entropy of the three-objective optimization. The optimal points that have been selected by the TOPSIS and the LINMAP decision making algorithms are exactly the same. While the fuzzy algorithm has achieved an optimal point with a slightly better entropy, it has a worse power function.

6.3.3 Two-objective optimization results

By having four objective functions, there could be six optimizations with two-objectives. Therefore, the Pareto frontier and the ultimate optimum results of each two-objective optimization are presented in Figs. 6–11 and Tables 8–13.

The results of the economic factor and the power of the two-objective optimization are exhibited in Fig. 6 and Table 8. According to these results, the fuzzy decision making algorithm has reached an optimal point with a

Table 3 Results of four-objective optimization with post-expression of preferences

	Decision variables					Objectives			
	φ	x	A_R	T_H	T_h	f	P	η	S
Fuzzy	1.003	0.4602	2.0689	1292.4	949.096	0.155	0.339	0.373	0.000395
LINMAP	1.0026	0.4802	4.1062	1391.2	907.0816	0.172	0.332	0.363	0.000401
TOPSIS	1.0411	0.4603	2.9210	1349.7	931.4148	0.183	0.337	0.351	0.000423

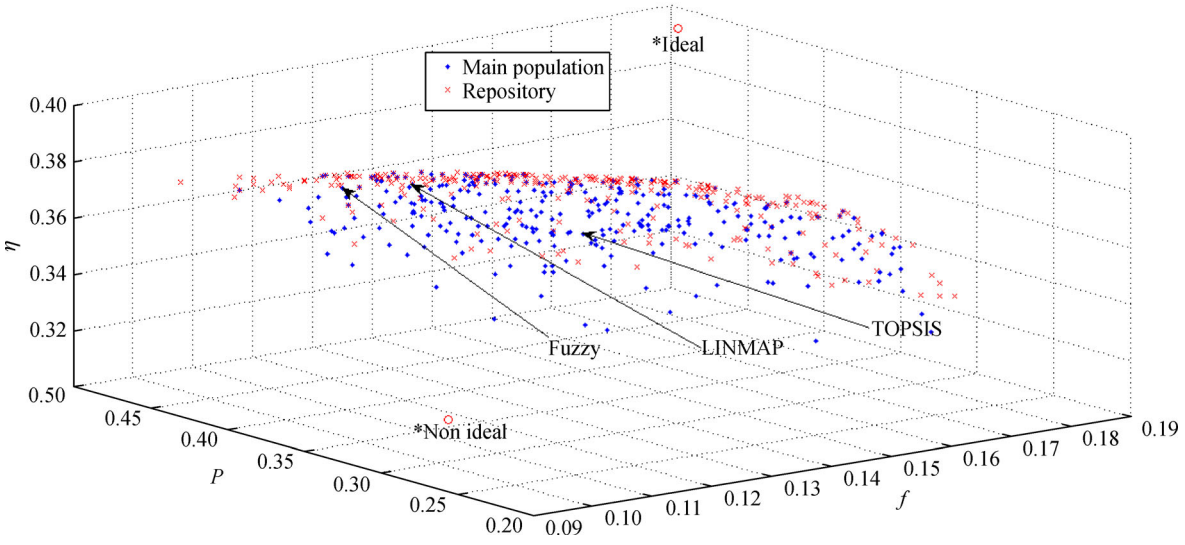

Fig. 2 Pareto frontier of three-objective (f, P, η) optimization with post-expression of preferences

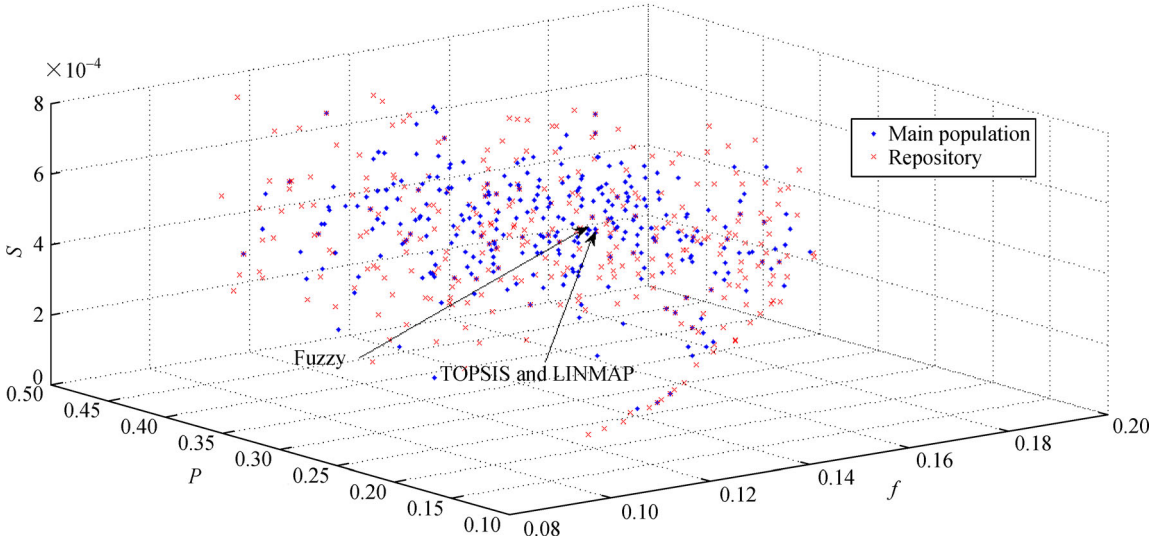

Fig. 3 Pareto frontier of three-objective (f, P, S) optimization with post-expression of preferences

Table 4 Results of three-objective (f, P, η) optimization with post-expression of preferences

	Decision variables					Objectives		
	φ	x	A_R	T_H	T_h	f	P	η
Fuzzy	1.0019	0.452	3.232	1286.2	932.82	0.145	0.423	0.364
LINMAP	1.0026	0.468	6.396	1310.2	897.80	0.158	0.431	0.355
TOPSIS	1.0303	0.475	5.061	1364.9	929.26	0.177	0.384	0.348

Table 5 Results of three-objective (f, P, S) optimization with post-expression of preferences

	Decision variables					Objectives		
	φ	x	A_R	T_H	T_h	f	P	η
Fuzzy	1.0031	0.4800	1.9688	1335.1	925.26	0.1412	0.357	0.000411
LINMAP	1.0080	0.4636	4.5553	1220.8	938.81	0.1629	0.341	0.000404
TOPSIS	1.0080	0.4636	4.5553	1220.8	938.81	0.1629	0.341	0.000404

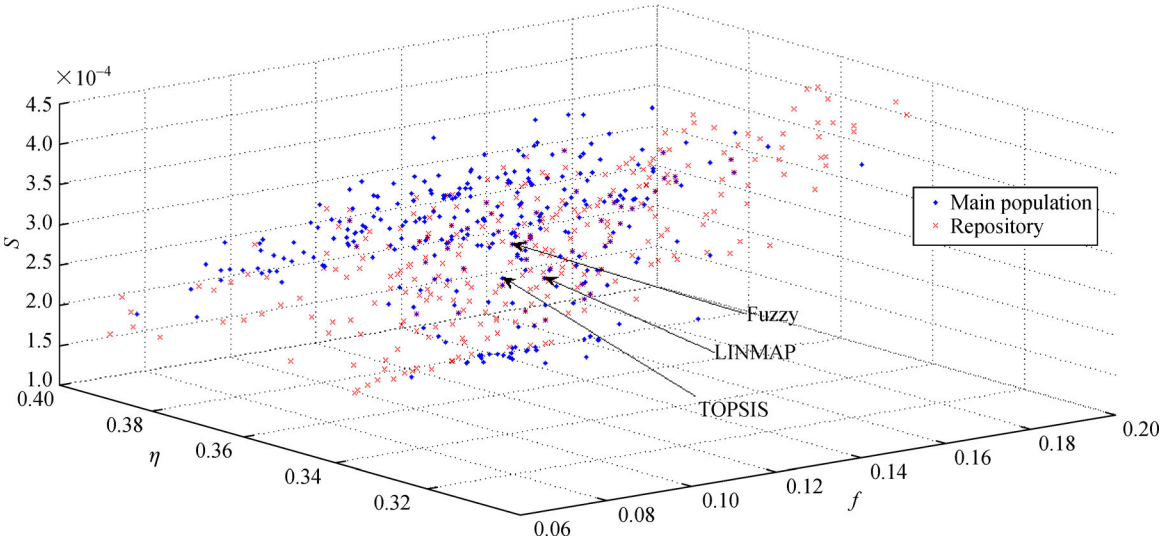

Fig. 4 Pareto frontier of three-objective (f, η, S) optimization with post-expression of preferences

Table 6 Results of three-objective (f, η, S) optimization with post-expression of preferences

	Decision variables					Objectives		
	φ	x	A_R	T_H	T_h	P	η	S
Fuzzy	1.0027	0.4750	2.4029	1229.5	974.21	0.1430	0.3784	0.000237
LINMAP	1.0171	0.4504	1.4500	1214.7	948.59	0.1426	0.3640	0.000213
TOPSIS	1.0014	0.4542	3.9563	1139.6	984.06	0.1415	0.3608	0.00208

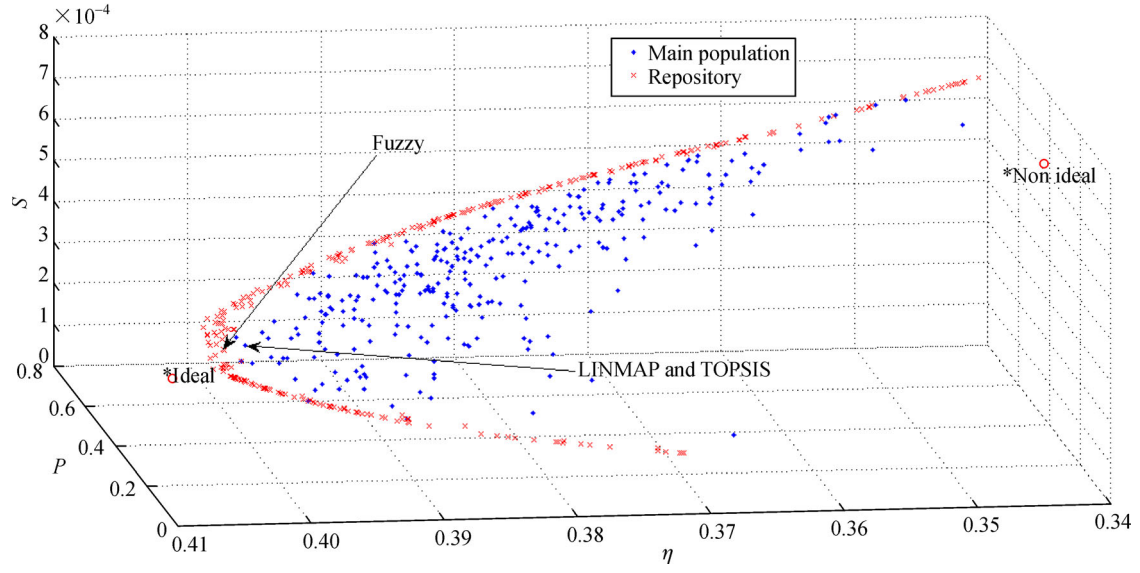

Fig. 5 Pareto frontier of three-objective (P, η, S) optimization with post-expression of preferences

higher power and the TOPSIS algorithm has reached a point with a higher economical factor. As tabulated in Table 8, in comparison with the other decision making algorithms, the optimal point chosen by the LINMAP algorithm is at a higher heat source temperature and a lower heat sink temperature.

In Fig. 7 and Table 9, the results of the economic factor and the thermal efficiency of the two-objective optimization are presented. Among the results of the three decision making algorithms, the ultimate optimal point of fuzzy

Table 7 Results of three-objective (P, η, S) optimization with post-expression of preferences

	Decision variables					Objectives		
	φ	x	A_R	T_H	T_h	P	η	S
Fuzzy	1.0054	0.4504	6.4309	1128.7	868.23	0.309	0.407	0.000280
LINMAP	1.0008	0.4503	7.9711	1137.7	850.00	0.315	0.407	0.000285
TOPSIS	1.0008	0.4503	7.9711	1137.7	850.00	0.315	0.407	0.000285

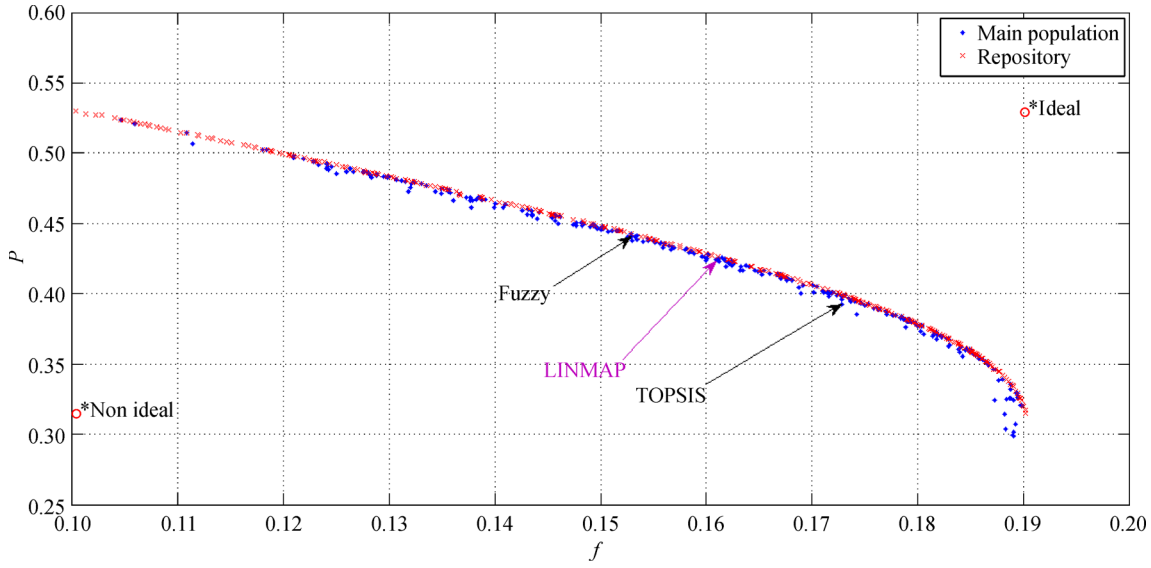

Fig. 6 Pareto frontier of two-objective (f, P) optimization with post-expression of preferences

Table 8 Results of two-objective (f, P) optimization with post-expression of preferences

	Decision variables					Objectives	
	φ	x	A_R	T_H	T_h	f	P
Fuzzy	1.0000	0.4726	3.0483	1399.9	945.86	0.1533	0.4423
LINMAP	1.0005	0.4836	4.1740	1400.0	929.26	0.1609	0.4275
TOPSIS	1.0002	0.4605	1.9859	1399.9	977.11	0.1738	0.3973

algorithm shows a better thermal efficiency but a lower economic factor, in comparison to the TOPSIS and the LINMAP algorithms. This optimal point has been in a lower amounts of x and A_R decision variable.

The results of the economic factor and the entropy of the two-objective optimization are represented in Fig. 9 and Table 11. The results show that the fuzzy decision making algorithm has selected a point with a better economic factor in comparison with the TOPSIS algorithm that reaches a point with a lower entropy change.

According to Fig. 10 and Table 12 which show the results of a two-objective optimization of the power and entropy, in order to reach the optimal point, all of the three decision making algorithms have reached a point with an

Table 9 Results of two-objective (f, η) optimization with post-expression of preferences

	Decision variables					Objectives	
	φ	x	A_R	T_H	T_h	f	η
Fuzzy	1.0003	0.4584	1.7197	1252.4	934.53	0.1500	0.3799
LINMAP	1.0005	0.4801	3.3165	1284.5	940.28	0.1812	0.3571
TOPSIS	1.0002	0.4750	3.0802	1326.8	965.14	0.1883	0.3507

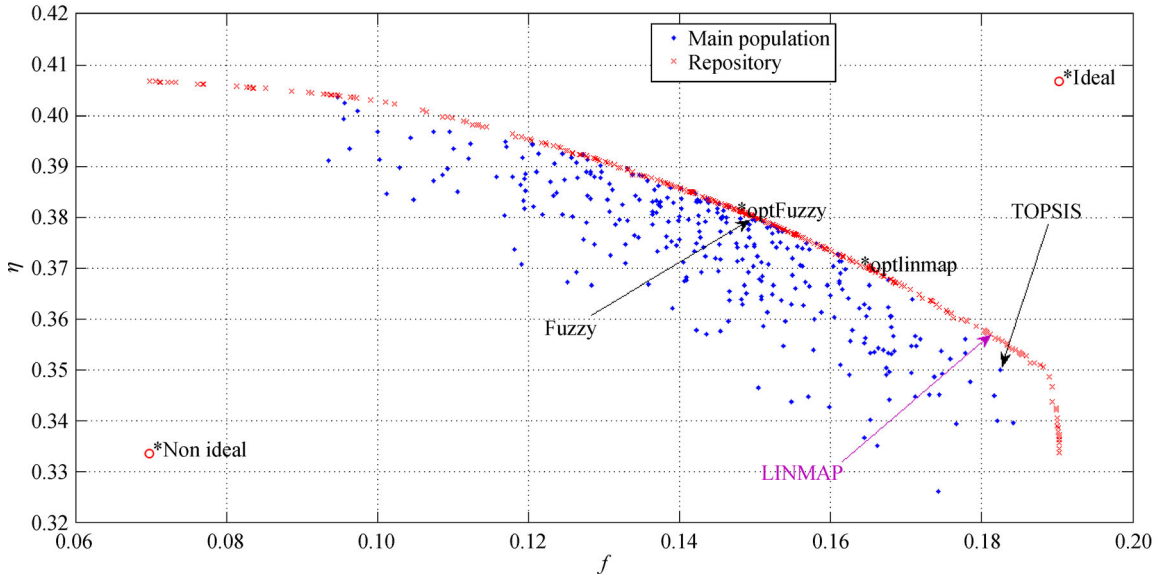

Fig. 7 Pareto frontier of two-objective (f, η) optimization with post-expression of preferences

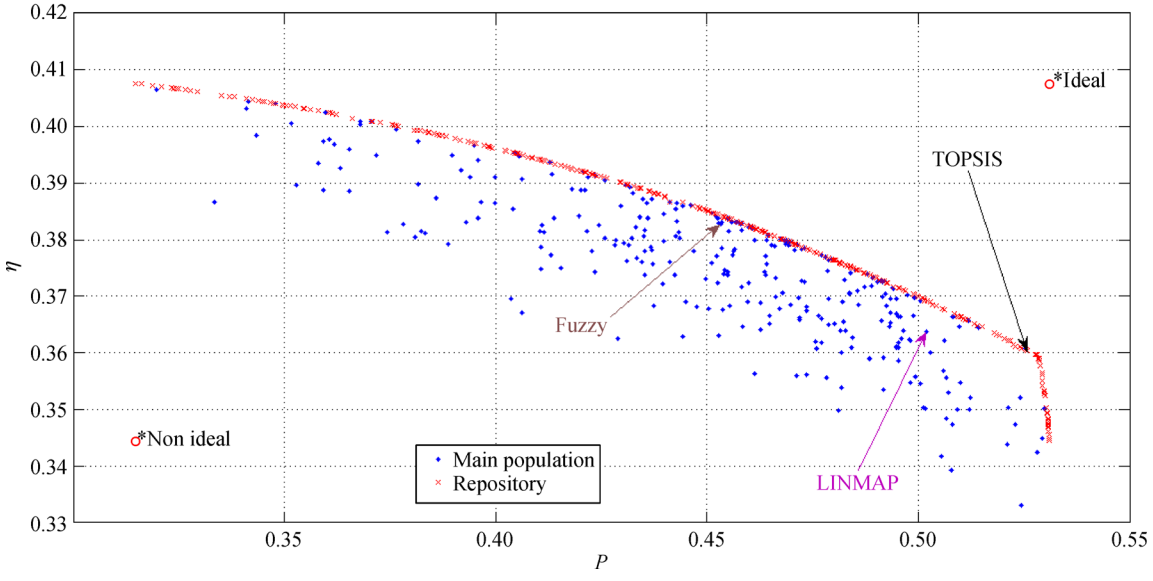

Fig. 8 Pareto frontier of two-objective (P, η) optimization with post-expression of preferences

Table 10 Results of two-objective (P, η) optimization with post-expression of preferences

	Decision variables					Objectives	
	φ	x	A_R	T_H	T_h	P	η
Fuzzy	1.0001	0.4520	9.9352	1152.3	852.47	0.4523	0.3845
LINMAP	1.0000	0.4542	9.9471	1299.5	858.50	0.5074	0.3674
TOPSIS	1.0000	0.4500	9.9586	1264.8	850.00	0.5283	0.3596

approximate maximum A_R (the cold side heat transfer area to the hot side heat transfer area). In comparison with other decision making algorithms, the fuzzy algorithm has selected an optimal point with a higher power and the TOPSIS algorithm has opted a point with a better entropy change.

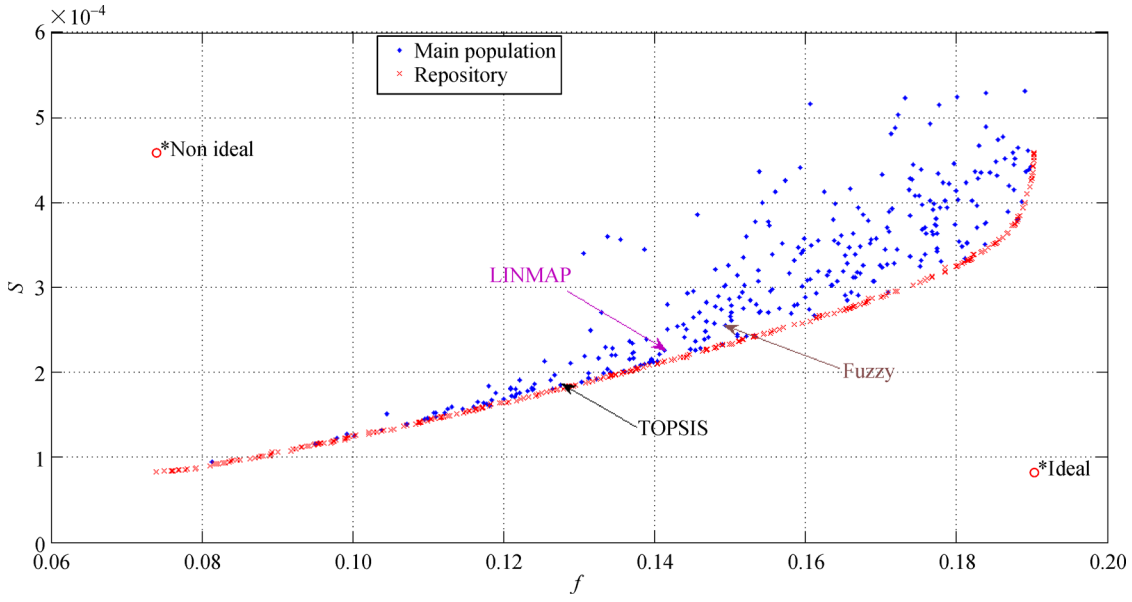

Fig. 9 Pareto frontier of two-objective (f, S) optimization with post-expression of preferences

Table 11 Results of two-objective (f, S) optimization with post-expression of preferences

	Decision variables					Objectives	
	φ	x	A_R	T_H	T_h	f	S
Fuzzy	1.0079	0.4500	0.7250	1240.2	984.29	0.1520	0.000235
LINMAP	1.0000	0.4519	0.5000	1276.9	960.01	0.1425	0.000211
TOPSIS	1.0007	0.4523	1.4500	1262.3	955.29	0.1275	0.000175

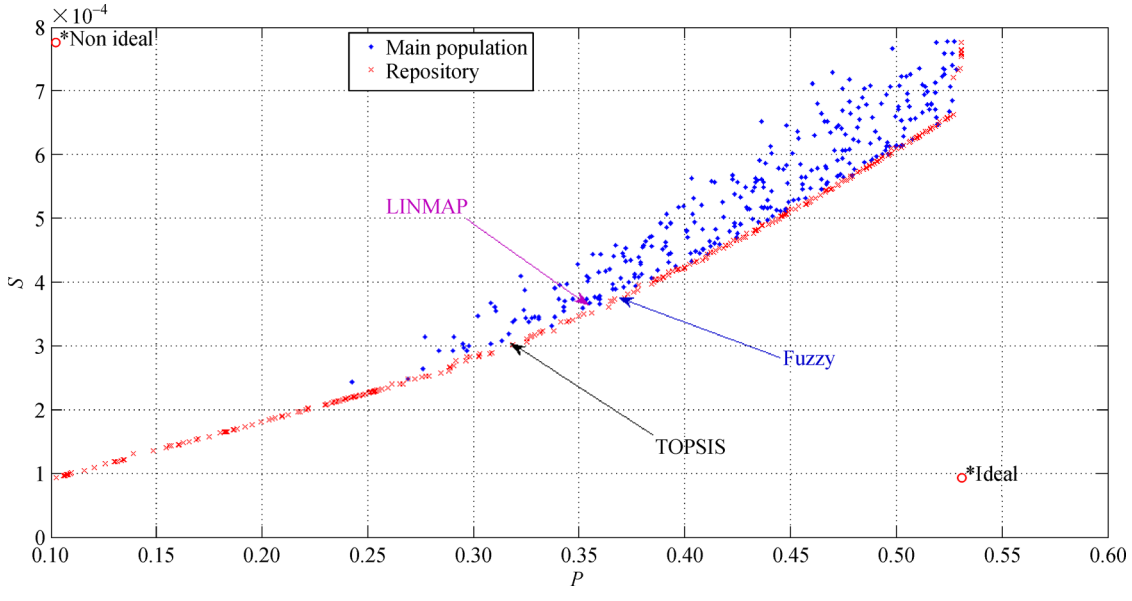

Fig. 10 Pareto frontier of two-objective (P, S) optimization with post-expression of preferences

Figure 11 and Table 13 represent the results of the thermal efficiency and the thermal efficiency of the two-objective optimization. The results show that the ultimate optimal points have been obtained at almost the minimum of x (the hot side temperature to the cold side temperature of the cycle), T_h (the hot side temperature) and T_H (the heat

Table 12 Results of two-objective (P, S) optimization with post-expression of preferences

	Decision variables					Objectives	
	φ	x	A_R	T_H	T_h	P	S
Fuzzy	1.0005	0.4816	9.6704	1339.3	857.53	0.3790	0.000391
LINMAP	1.0000	0.4711	9.3228	1209.7	865.87	0.3571	0.000358
TOPSIS	1.0059	0.4929	10.0000	1377.8	850.00	0.3227	0.000308

source temperature). According to Table 13, the fuzzy decision making algorithm has chosen a point with a higher thermal efficiency and the TOPSIS algorithm has selected a point with a better entropy change.

6.4 Validation

Apart from the various optimizations done in this work, some optimizations have been done in some other papers. Therefore, the results of optimizations in these papers can be verified with some references. According to the results of single-objective optimization, in order to achieve the optimal thermal efficiency, the heat source temperature should be about 1100°C. As shown in Fig. 12, similar results were reported in Refs. [22,23] in a wide range of the concentration ratios. In addition, among the decision variables, x (the hot side temperature to the cold side temperature of the cycle) is in a range of 0.45 to 0.50 that can be verified by the results from Refs. [23,25]. Figure 13 shows the range of the optimum point for variable x.

Also, as shown in Fig. 13, the optimal thermal efficiency results obtained through various multi-objective optimizations in this research are in a range of 0.35% to 0.41% which is a valid range for a Stirling cycle thermal efficiency [30].

Therefore, the validation can be presented in brief as shown in Table 14.

It also shows that, with a finite time analysis of a dish-Stirling cycle and by implementing the irreversibility factor, the MOPSO multi-objective optimization can lead

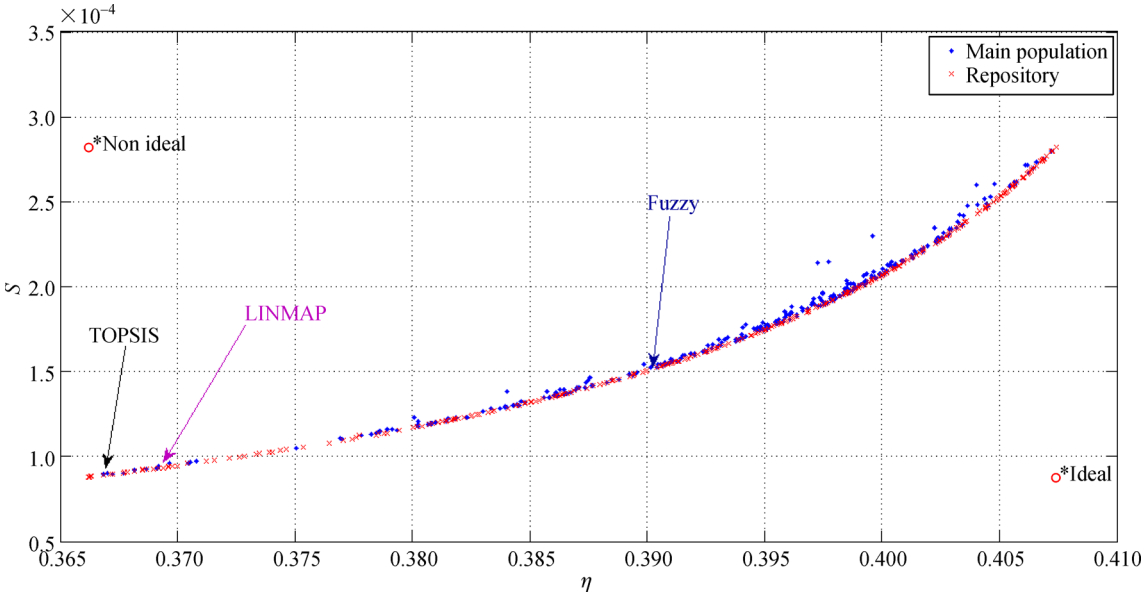

Fig. 11 Pareto frontier of two-objective (η, S) optimization with post-expression of preferences

Table 13 Results of two-objective (η, S) optimization with post-expression of preferences

	Decision variables					Objectives	
	φ	x	A_R	T_H	T_h	η	S
Fuzzy	1.0000	0.4502	1.9978	1100.2	853.18	0.3903	0.000152
LINMAP	1.0000	0.4500	2.5461	1100.6	865.72	0.3686	0.000092
TOPSIS	1.0005	0.4502	4.5771	1100.9	859.37	0.3618	0.000118

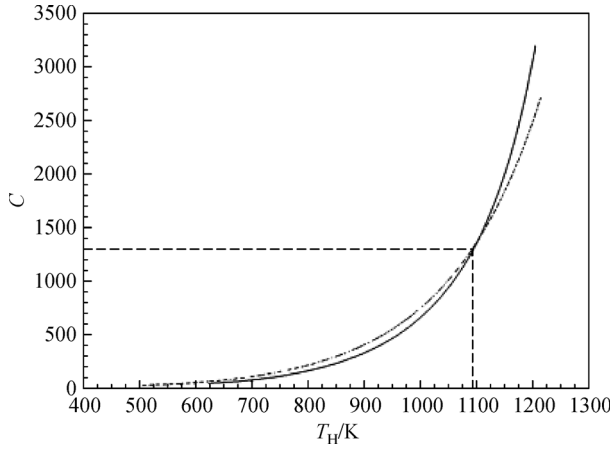

Fig. 12 Optimum absorber temperature and concentrating ratio of the system (Adapted with permission from Ref. [22])

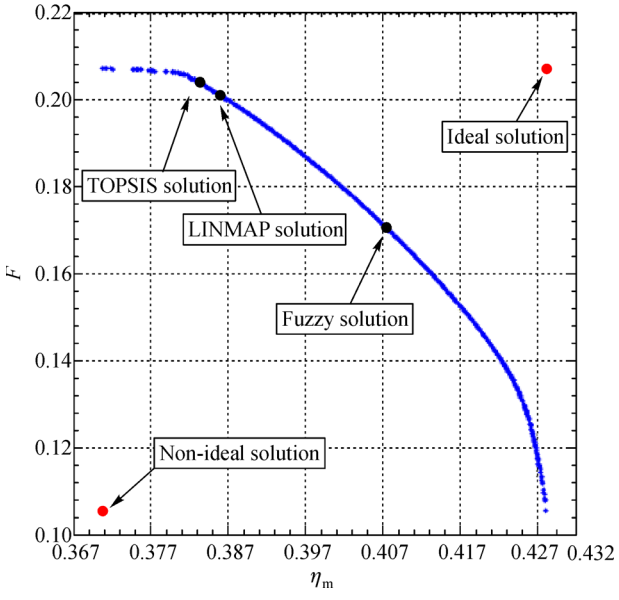

Fig. 13 Pareto optimal frontier in objectives' space (thermal efficiency- dimensionless objective function)

Table 14 Verification of decision variables of x and T_H [22,30]

Decision variable or objective function	In this paper	In the references
T_H	1100	1100
η_m	0.35 < < 0.40	0.37 < < 0.41

to an acceptable series of results, which represent the characteristics of a real system.

7 Conclusions

For the first time in a dish-Stirling finite time analysis, a four-objective optimization of the economic factor, the power, the thermal efficiency, and the entropy change are implemented and for optimization, the MOPSO algorithm has been used. A series of results can be achieved by a series of the multi-objective optimizations done in this research. According to the results of the four-objective optimization at the ultimate optimal point, the dimensionless power is in the range of 0.33 to 0.34 and the thermal efficiency is opted in the range of 0.35 to 0.37. Among the decision making methods, the fuzzy method has chosen an optimal point with the best thermal efficiency and slightly more optimum entropy, while an optimal point with a better economical factor has been obtained by the TOPSIS method. In this investigation, the results of the single-objective and multi-objective optimization of the dish-Stirling cycle can be a reference for further studies. In addition, the adaptation of the results with practical works demonstrates the applicability of finite time analysis at estimating a dish-Stirling system performance.

Acknowledgements This research was supported by the Scientific Research Foundation of Wuhan University of Technology (No. 40120237), the ESI Discipline Promotion Foundation of WUT (No.35400664).

Notations

A_{res}	Absorber area
A_{app}	Aperture area
C	Concentration ratio
F	Dimensionless objective function
f	Dimensionless economic factor
h	Heat transfer coefficient/(W·K^{-4} or W·m^{-2}·K^{-1})
I	Direct solar flux intensity/(W·m^{-2})
i	ith objective
j	jth solution
n	Mole number of the working fluid/mol
P	Dimensionless output power
Q	Heat transfer/J
R	Universal gas constant/(J·mol^{-1}·K^{-1})
S	Dimensionless entropy
T	Temperature/K
W	Work/J
V	Volume
t	Cyclic period/s
x	Temperature ratio of the Stirling engine
Greek letters	
λ	Ratio of volume during the regenerative processes
η	Thermal efficiency
ε	Emissivity factor
σ	Entropy

δ	Stefan–Boltzmann coefficient
Subscripts	
H	Absorber (heater)
h	High temperature side heat exchanger
L	Heat sink
c	Low temperature side heat exchanger
m	Entire solar dish Stirling system
t	Stirling engine
0	Ambient condition, optics
1–4	Process states

References

1. EIA. International Energy outlook. 2011–09, available at the website of eia. gov
2. Curzon F L, Ahlborn B. Efficiency of a Carnot engine at maximum power output. American Journal of Physics, 1975, 43(1): 22–24
3. Moran M J. On second law analysis and the failed promises of finite time thermodynamics. Energy, 1998, 23(6): 517–519
4. Gyftopoulos E P. Fundamentals of analysis of processes. Energy Conversion and Management, 1997, 38(15–17): 1525–1533
5. Tlili I, Timoumi Y, Nasrallah S B. Thermodynamic analysis of the Stirling heat engine with regenerative losses and internal irreversibilities. International Journal of Engine Research, 2008, 9(1): 45–56
6. Kaushik S C, Kumar S. Finite time thermodynamic evaluation of irreversible Ericsson and Stirling heat engines. Energy Conversion and Management, 2001, 42(3): 295–312
7. Kaushik S C, Kumar S. Finite time thermodynamic analysis of endoreversible Stirling heat engine with regenerative losses. Energy, 2000, 25(10): 989–1003
8. Kaushik S C, Tyagi S K, Bose S K, Singhal M K. Performance evaluation of irreversible Stirling and Ericsson heat pump cycles. International Journal of Thermal Sciences, 2002, 41(2): 193–200
9. Costea M, Petrescu S, Harman C. The effect of irreversibilities on solar Stirling engine cycle performance. Energy Conversion and Management, 1999, 40(15–16): 1723–1731
10. Urieli I, Kushnir M. The ideal adiabatic cycle-a rational basis for Stirling engine analysis. In: Proceeding of 17th IECEC, Los Angeles, CA, USA, 1982
11. Wu F, Chen L, Wu C, Sun F. Optimum performance of irreversible Stirling engine with imperfect regeneration. Energy Conversion and Management, 1998, 39(8): 727–732
12. Petrescu S, Costea M, Harman C, Florea T. Application of the direct method to irreversible Stirling cycles with finite speed. International Journal of Energy Research, 2002, 26(7): 589–609
13. Timoumi Y, Tlili I, Ben Nasrallah S. Design and performance optimization of GPU-3 Stirling engines. Energy, 2008, 33(7): 1100–1114
14. Cheng C H, Yu Y J. Numerical model for predicting thermodynamic cycle and thermal efficiency of a beta-type Stirling engine with rhombic-drive mechanism. Renewable Energy, 2010, 35(11): 2590–2601
15. Ataer O E. Numerical analysis of regenerators of piston type Stirling engines using Lagrangian formulation. International Journal of Refrigeration, 2002, 25(5): 640–652
16. Tlili I. Finite time thermodynamic evaluation of endoreversible Stirling heat engine at maximum power conditions. Renewable & Sustainable Energy Reviews, 2012, 16(4): 2234–2241
17. Formosa F, Despesse G. Analytical model for Stirling cycle machine design. Energy Conversion and Management, 2010, 51(10): 1855–1863
18. Formosa F. Coupled thermodynamic-dynamic semi-analytical model of free piston Stirling engines. Energy Conversion and Management, 2011, 52(5): 2098–2109
19. Iwamoto I, Toda K, Hirata K, Takeuchi M, Yamamoto T. Comparison of low and high temperature differential Stirling engines. In: Proceedings of the 8th International Stirling engine conference, Anacona, Italy, 1997
20. Ahmadi M H, Hosseinzade H. Investigation of solar collector design parameters effect onto solar Stirling engine efficiency. Journal of Applied Mechanical Engineering, 2012, 1(01): 1–4
21. Erbay L B, Yavuz H. Analysis of Stirling heat engine at maximum power conditions. Energy, 1997, 22(7): 645–650
22. Li Y, He Y L, Wang W W. Optimization of solar-powered Stirling heat engine with finite-time thermodynamics. Renewable Energy, 2011, 36(1): 421–427
23. Sharma A, Shukla S K, Rai A K. Finite time thermodynamic analysis and optimization of Solar-Dish Stirling heat engine with regenerative losses. Thermal Science, 2011, 15(4): 995–1009
24. Sayyaadi H. Multi-objective approach in thermoenvironomic optimization of a benchmark cogeneration system. Applied Energy, 2009, 86(6): 867–879
25. Ahmadi M H, Sayyaadi H, Dehghani S, Hosseinzade H. Designing a solar powered Stirling heat engine based on multiple criteria: maximized thermal efficiency and power. Energy Conversion and Management, 2013, 75: 282–291
26. Chen C, Ho C, Yau H. Performance analysis and optimization of a solar powered Stirling engine with heat transfer considerations. Energies, 2012, 5(12): 3573–3585
27. Jafari S, Mohammadi B, Boroujerdi A A. Multi-objective optimization of a Stirling-type pulse tube refrigerator. Cryogenics, 2013, 55–56: 53–62
28. Ahmadi M H, Mohammadi A H, Dehghani S, Barranco-Jiménez M. Multi-objective thermodynamic-based optimization of output power of solar dish-Stirling engine by implementing an evolutionary algorithm. Energy Conversion and Management, 2013, 75: 438–445
29. Ahmadi M H, Hosseinzade H, Sayyaadi H, Mohammadi A H, Kimiaghalam F. Application of the multi-objective optimization method for designing a powered Stirling g heat engine: design with maximized power, thermal efficiency and minimized pressure loss. Renewable Energy, 2013, 60: 313–322
30. Ahmadi M H, Sayyaadi H, Mohammadi A H, Barranco-Jiménez M. Thermo-economic multi-objective optimization of solar dish-Stirling engine by implementing evolutionary algorithm. Energy Conversion and Management, 2013, 73: 370–380
31. Lazzaretto A, Toffolo A. Energy, economy and environment as objectives in multi-criterion optimization of thermal systems design. Energy, 2004, 29(8): 1139–1157

32. Ahmadi M H, Ahmadi M A, Mohammadi A H, Feidt M, Pourkiaei S M. Multi-objective optimization of an irreversible Stirling cryogenic refrigerator cycle. Energy Conversion and Management, 2014, 82: 351–360
33. Chaitou H, Nika P. Exergetic optimization of a thermoacoustic engine using the particle swarm optimization method. Energy Conversion and Management, 2012, 55: 71–80
34. Duan C, Wang X, Shu S, Jing C, Chang H. Thermodynamic design of Stirling engine using multi-objective particle swarm optimization algorithm. Energy Conversion and Management, 2014, 84: 88–96
35. Toghyani S, Kasaeian A, Ahmadi M H. Multi-objective optimization of Stirling engine using non-ideal adiabatic method. Energy Conversion and Management, 2014, 80: 54–62
36. Ahmadi M H, Mehrpooya M, Pourfayaz F. Exergoeconomic analysis and multi objective optimization of performance of a carbon dioxide power cycle driven by geothermal energy with liquefied natural gas as its heat sink. Energy Conversion and Management, 2016, 119: 422–434
37. Ahmadi M H, Ahmadi M A, Mellit A, Pourfayaz F, Feidt M. Thermodynamic analysis and multi objective optimization of performance of solar dish Stirling engine by the centrality of entransy and entropy generation. International Journal of Electrical Power & Energy Systems, 2016, 78: 88–95
38. Ahmadi M H, Ahmadi M A, Feidt M. Thermodynamic analysis and evolutionary algorithm based on multi-objective optimization of performance for irreversible four-temperature-level refrigeration. Mechanics & Industry, 2015, 16(2): 207
39. Kennedy J, Eberhart R. Particle swarm optimization. In: Proceeding of International Conference on Neural Networks. Perth, Australia, 1995